NeuroImage 187 (2019) 3–16

Contents lists available at ScienceDirect

NeuroImage

journal homepage: www.elsevier.com/locate/neuroimage

Recent progress in ASL

Luis Hernandez-Garcia *, Anish Lahiri, Jonas Schollenberger

FMRI Laboratory, University of Michigan, United States

A B S T R A C T

This article aims to provide the reader with an overview of recent developments in Arterial Spin Labeling (ASL) MRI techniques. A great deal of progress has been made in recent years in terms of the SNR and acquisition speed. New strategies have been introduced to improve labeling efficiency, reduce artefacts, and estimate other relevant physiological parameters besides perfusion. As a result, ASL techniques has become a reliable workhorse for researchers as well as clinicians. After a brief overview of the technique's fundamentals, this article will review new trends and variants in ASL including vascular territory mapping and velocity selective ASL, as well as arterial blood volume imaging techniques. This article will also review recent processing techniques to reduce partial volume effects and physiological noise. Next the article will examine how ASL techniques can be leveraged to calculate additional physiological parameters beyond perfusion and finally, it will review a few recent applications of ASL in the literature.

Introduction

A major goal of modern medical imaging is to move beyond qualitative images that may be informative about the shape, size and texture of tissue, and into a world where medical images are also quantitative. One of the more popular and prominent techniques is arterial spin labeling (ASL), which can produce quantitative images of perfusion. Brain perfusion (defined as the amount of blood delivered to a unit of tissue per unit of time) is a well known indicator of tissue metabolism and function. As such, it is proving to be a powerful workhorse to study brain function and gaining prominence as a clinical tool, but it is still an evolving technique.

The concept behind ASL is relatively simple: conceptually, it is very similar to tracer injection perfusion measurements (e.g., bolus tracking MRI, autoradiography, PET … etc.) except that, instead of injecting a tracer into the blood stream and tracking its accumulation into the tissue, the tracer consists of the blood water in the arteries itself. The tracer is created by inverting the magnetization of the blood in the arteries that feed the organ of interest with a train of RF pulses. As this "labeled" blood flows into the tissue, it reduces the available magnetization in the tissue. As a result, images collected downstream of the labeling location appear slightly darker. By subtracting the labeled images from a set of control images, we can calculate the amount of blood that entered the organ since the beginning of the labeling period. For example, the most common use of ASL is for brain perfusion imaging, is done by labeling blood just before it enters the brain through the carotid and vertebral arteries. After a brief delay, a set of "labeled" brain images is acquired. Next, a second set of "control" images is acquired identical to the first, except that this time, the labeling pulses do not invert the blood magnetization at all, but simply serve as a control for any side effects of the labeling pulses (namely magnetization transfer (Williams et al., 1992; Wolff and Balaban, 1989; Zhang et al., 1995)). The subtraction of these two images is roughly proportional to the perfusion rate (see Fig. 1, depicting the ASL technique). If desired, one can acquire a time series of such image pairs in order to examine the brain's activity during a stimulation paradigm.

The main variations of the technique have to do with the labeling scheme. One could label a large segment of the neck region with a single pulse, as in the case of Pulsed ASL techniques, or one could apply a long pulse (or a train of pulses) at a thin slice through the neck that labels the blood as it flows through it, as in the case of continuous and pseudo-continuous ASL. More recently, "velocity selective" techniques have been developed such that only moving spins are labeled, regardless of their spatial position.

In general, ASL subtraction images have been shown to be roughly proportional to the perfusion rate with the appropriate scaling factors for the specific technique. Since the invention of ASL, there have been numerous validation studies of different ASL variants and their corresponding quantification models that compared them to other independent perfusion measurements (Chappell et al., 2013; Chen et al., 2008; Ewing et al., 2005; Gao et al., 2014; Hartkamp et al., 2014; Ye, 2000).

While ASL was invented around the same time as the BOLD effect was discovered (Detre et al., 1992; Williams et al., 1992), it has only been in the last five years that ASL has been widely adopted by the neuroimaging community. Largely, this recent resurgence of ASL has come about

* Corresponding author. FMRI Laboratory, University of Michigan, 2360 Bonisteel Blvd., Ann Arbor, MI 48109-2108, United States.
E-mail address: hernan@umich.edu (L. Hernandez-Garcia).

https://doi.org/10.1016/j.neuroimage.2017.12.095
Received 30 September 2017; Received in revised form 21 December 2017; Accepted 30 December 2017
Available online 3 January 2018

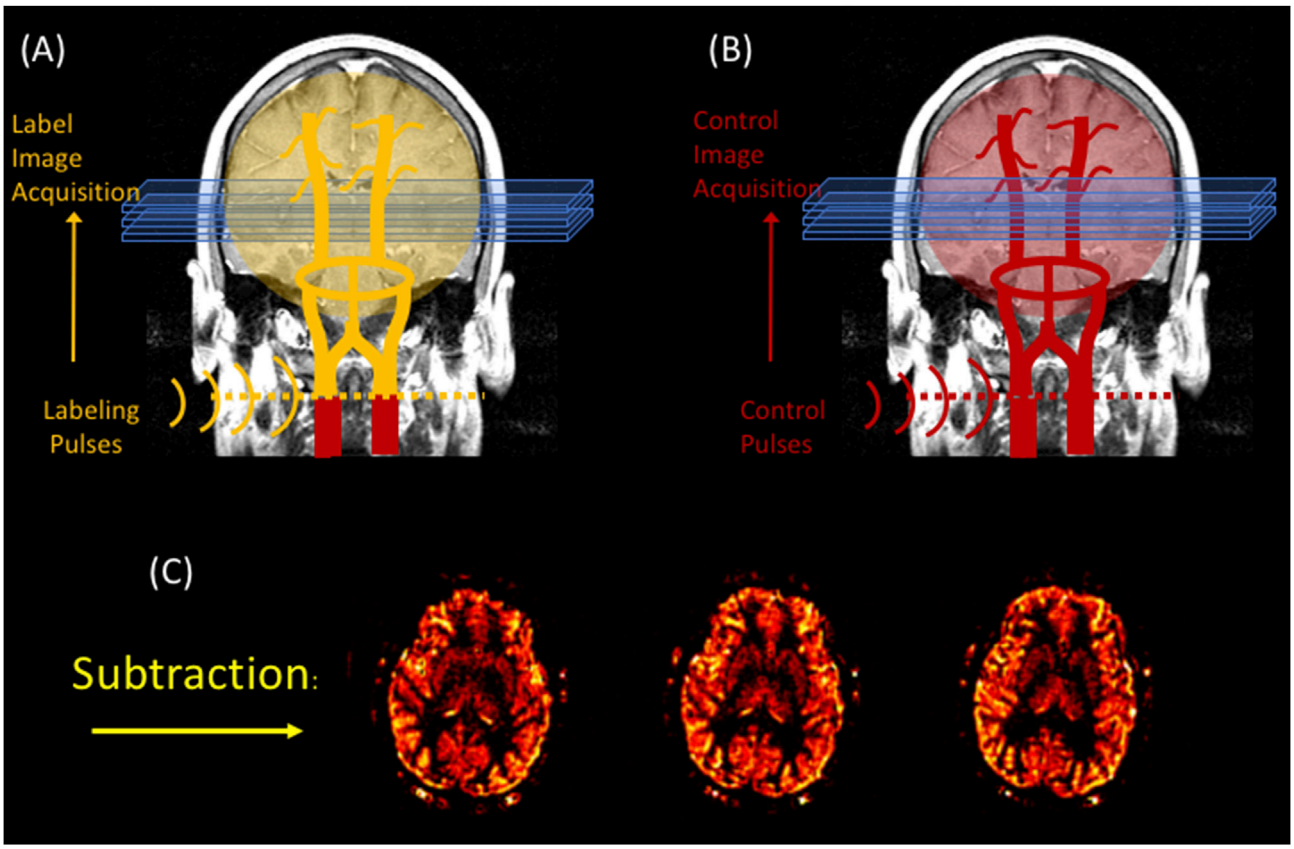

Fig. 1. A basic pseudo-continuous ASL experiment. The arterial water is inverted as it crosses a plane through the neck prior to acquiring the "labeled" image. A second "control" image is acquired without the label. The subtraction of these two images yields a perfusion weighted image.

because of a combination of technical advances. The technique was previously challenged by its inherent low signal to noise ratio (SNR), and slow temporal resolution. With the advent of parallel imaging (Blaimer et al., 2004; Deshmane et al., 2012; Pruessmann et al., 1999), the development of pseudo-continuous labeling (Dai et al., 2008) and background suppression schemes (Ye et al., 2000; St. Lawrence et al., 2005; Garcia et al., 2005), ASL images can now be acquired with sufficient speed and quality to be a robust, quantitative imaging tool. Another major hurdle to the adoption of ASL was the great diversity of schemes used by different investigators. It was not until 2014, that the community came together to make a set of recommendations for the implementation of a robust variant of ASL that could be used reliably as a "standard" implementation, even if not necessarily the best possible implementation for every application. However, this has created a *de facto* standard and helped the different vendors implement an ASL pulse sequence that can be distributed as a packaged product (Alsop et al., 2015). At the time of this writing, there are efforts under way to establish gold standards for calibration and validation of ASL images. Specifically, a profile for ASL is being created for the Quantitative Imaging Biomarkers Alliance (QIBA see http://www.rsna.org/qiba) that will describe a set of applications, capabilities and standards for ASL as a quantitative biomarker.

Having said that, this article will focus on recent progress in the development of ASL techniques at the time of writing. As mentioned earlier, a great deal of progress has been made in recent years on fast image acquisition techniques to boost the SNR and speed of the measurement. Additionally, new strategies have been introduced to improve labeling efficiency, reduce artefacts, and estimate other relevant physiological parameters using ASL techniques besides perfusion. As a result, a host of new applications for ASL techniques is becoming available to researchers, although we will only focus on neuroimaging applications.

Velocity and acceleration selective labeling

The main challenges faced by ASL are its low signal to noise ratio (SNR) and its slow temporal and spatial resolution (Chen et al., 2011; Perthen et al., 2008; Wong et al., 1998). The low SNR is due in part to the small fraction of blood that enters a voxel. Additionally, by the time the labeled spins reach the voxel, they have relaxed significantly during transit. T1 relaxation during bolus arrival time destroys about 50% of the label. The longer the travel time, the more label is lost. The SNR challenge is most significant in the white matter (Van Gelderen et al., 2008) where perfusion rates are lower and arterial bolus arrival times are longer. Although feasible (Van Osch et al., 2009), white matter ASL imaging requires lengthy scans and yields images of inferior quality. As a result, white matter perfusion is often neglected or overlooked.

A solution to this problem was proposed in 1999, by the introduction of velocity-selective saturation pulses (Norris and Schwarzbauer, 1999) and demonstrated in humans (Wong et al., 2006; Wu and Wong, 2007). The concept is relatively simple: instead of inverting the spins at the feeding arteries, upstream of the target region, an arterial label can also be created *within the target region* by saturating only the moving spins (i.e., blood), thus reducing the arrival time of the label to a negligible amount. The arterial saturation was originally achieved by a 90° pulse that first tips the magnetization into the transverse plane, followed by two or more adiabatic 180° pulses surrounded by gradient pulses with a net zero moment. This results in dephasing of spins moving above a certain velocity encoding threshold, or Venc, while the spins moving slower than the threshold regain phase coherence. Lastly, the magnetization is returned to the z-axis by a −90° pulse. Ideally, after this preparation pulse train, the arterial and venous spins are saturated while the stationary tissue spins are largely unaffected (see Fig. 2). In order to produce a suitable control image, the same preparation pulse train is played out

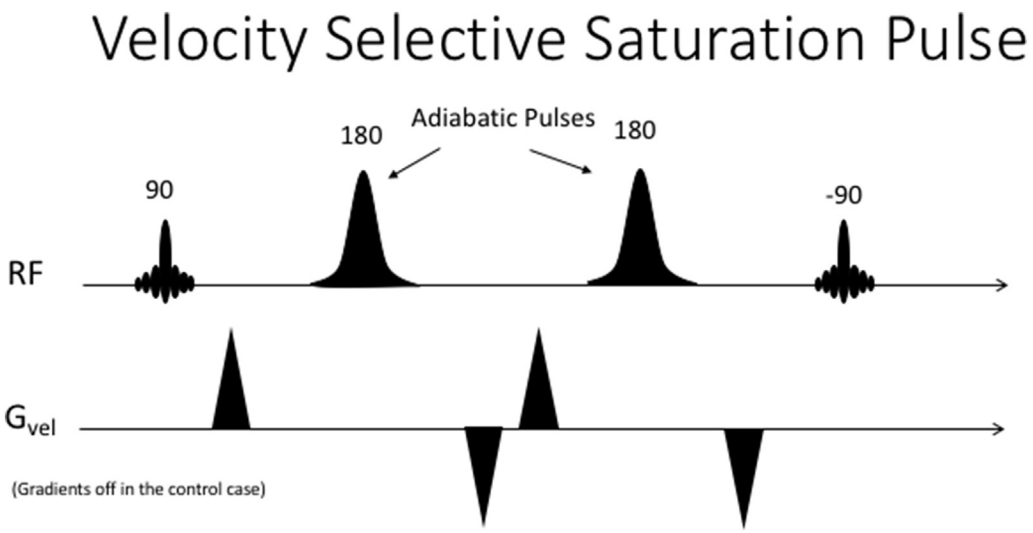

Fig. 2. A basic velocity selective labeling pulse train.

again, but without the velocity encoding gradients, thus returning all the spins to the longitudinal axis. It's important to note that this preparation will be very sensitive to the flip angles obtained with each individual pulse, thus most implementations will use adiabatic pulses, which are known to be more robust to B1 inhomogeneity.

There are some drawbacks to this strategy. First, the label consisted in saturation of the arterial spins, rather than inversion, thus giving up half of the label. Second, the velocity encoding gradients generate unwanted eddy currents and diffusion weighting in the labeled image that are not present in the control image. After subtracting control and labeled images, these effects result in systematic bias in a perfusion measure. The diffusion sensitivity issue results can be particularly noticeable because the ASL subtraction image can potentially show large signals arising from the cerebrospinal fluid, completely unrelated to perfusion. Finally, the size of the labeling bolus (or input function) is not as large as in the PCASL case, reducing the SNR of the measurement.

However, steady progress has been made to alleviate these problems starting with the inclusion of adiabatic pulses (Wong et al., 2006; Wu and Wong, 2007). Using a cleverly designed composite BIR-8 pulse train (see Fig. 3), Guo and Meakin were able to reduce the eddy current and diffusion effects (Guo et al., 2014; Meakin and Jezzard, 2013) quite dramatically. Further inroads have been made by concatenating two or three such labeling pulses in order to achieve a significantly longer labeling input function and boost the SNR of the resulting ASL image (Guo et al., 2014).

Recently, Qin et al., have introduced a composite pulse train that inverts the magnetization of spins moving within a velocity band, while leaving the magnetization of other velocities largely intact. This pulse train is based on a velocity phase-encoding formalism, analogous to k-space excitation (see Fig. 4). One can think of it as traversing velocity k-space with a hard 180° pulse that is broken into equal segments. An additional set of refocusing 180° pulses is added to refocus off-resonance effects along the way. As a result, they demonstrated that the technique could produce ASL images rivaling PCASL in terms of SNR, but without the sensitivity to bolus arrival time variations. This group has also been able to dramatically improve the quality of non-contrast angiography using this technique (Qin et al., 2015; Qin and van Zijl, 2016).

An interesting issue in velocity selective labeling is that arterial blood is known to decelerate significantly as it enters the brain. This can lead to some challenges (i.e., errors in velocity selectivity) but also opportunities. Using a similar strategy to velocity encoding, acceleration selective labeling was demonstrated by Schmid et al. (Obara et al., 2016; Schmid et al., 2014, 2015). Acceleration encoding can be done using similar principles as in the velocity encoding case, but the encoding is done by designing the gradient pulses such that their zeroth and their first order moments equal zero. In the case of the original implementation by Schmid et al. (2014), converting the pulse from velocity to acceleration selective was just a matter of reversing the sign of two of the gradient lobes.

Velocity and Acceleration selective labeling are, at the time of writing, still areas of active research and development and we expect to see new variants and applications in the near future.

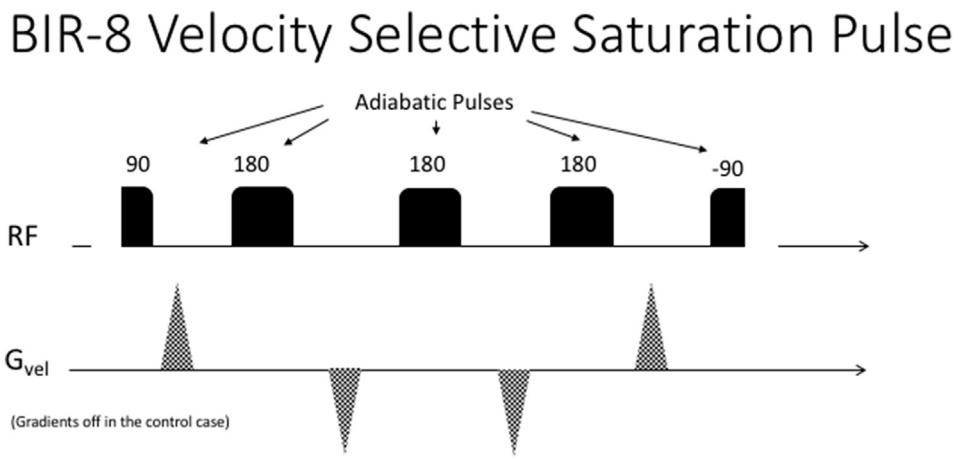

Fig. 3. Velocity Selective Saturation pulses using a BIR-8 scheme in order to reduce eddy current artefacts. In the control case, the velocity selective gradients are turned off.

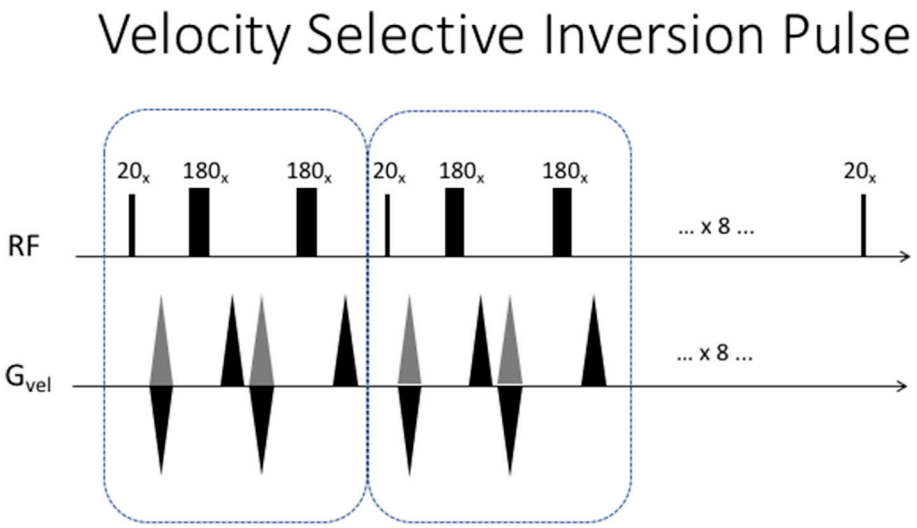

Fig. 4. Velocity Selective Inversion pulse described by Qin et al. A 180° hard pulse is broken into nine 20° segments. Additional 180's are interspersed to refocus off-resonance effects and correct for B1 inhomogeneity. These follow an MLEV phase pattern. In the control case, the velocity selective gradients are always positive (shown in grey).

Vascular territory imaging (VTI)

Knowledge of cerebral perfusion territories can provide significant information in clinical cases where the vascular tree is compromised (e.g. carotid stenosis, intracranial arteriovenous malformation) and knowledge of collateral blood supply to each region is necessary. "Vessel-selective" labeling can be achieved by modifying the PCASL scheme to invert only the blood traveling through specific sub-regions of the labeling plane. A recent example of vessel selective ASL can be seen in a study by Richter et al., in which the technique was used to examine the reorganization of blood flow supply following steno-occlusive disease (Richter et al., 2017). Currently available approaches of VTI generally rely on the application of additional gradient pulses along the labeling plane between RF pulses, in combination with a linear phase shift to the RF pulse train (see Fig. 5). The additional in-plane gradients cause flowing spins to accumulate an extra phase shift, $\Delta\phi$, depending on their location within the labeling plane:

$$\Delta\phi_k = \gamma\left(G_{z,ave}\cdot z\cdot\Delta t + G_{0,x,k}\cdot x + G_{0,y,k}\cdot y\right) \quad (1)$$

Where γ is the gyromagnetic ratio; $G_{z,ave}$ is the mean slice-selective gradient; $G_{0,x,k}$ and $G_{0,y,k}$ are the zeroth moments of the transverse x- and y gradients at the kth RF pulse; x, y, and z denote the label position relative to the isocenter. The phase of the next RF pulse must then be adjusted to match the phase gain at the desired location. As a result, only spins in the desired location (with the right amount of phase) maintain the spin lock condition and become inverted.

Vessel-encoded pcasl (ve-pcasl), as first introduced by Wong (2007), uses constant gradients to generate a periodic banding pattern along the labeling plane where the flowing spins are inverted. Thus, two separate vessels can be in a tag and a control region, respectively by adjusting the in-plane gradient such that there is a 180° phase shift between them (see the left panel of Fig. 6). By extension of this concept, a Hadamard encoding scheme can be used to label different combinations of vessels over several ASL image acquisitions. The perfusion contributions from individual vessels to each voxel can be calculated from the resulting

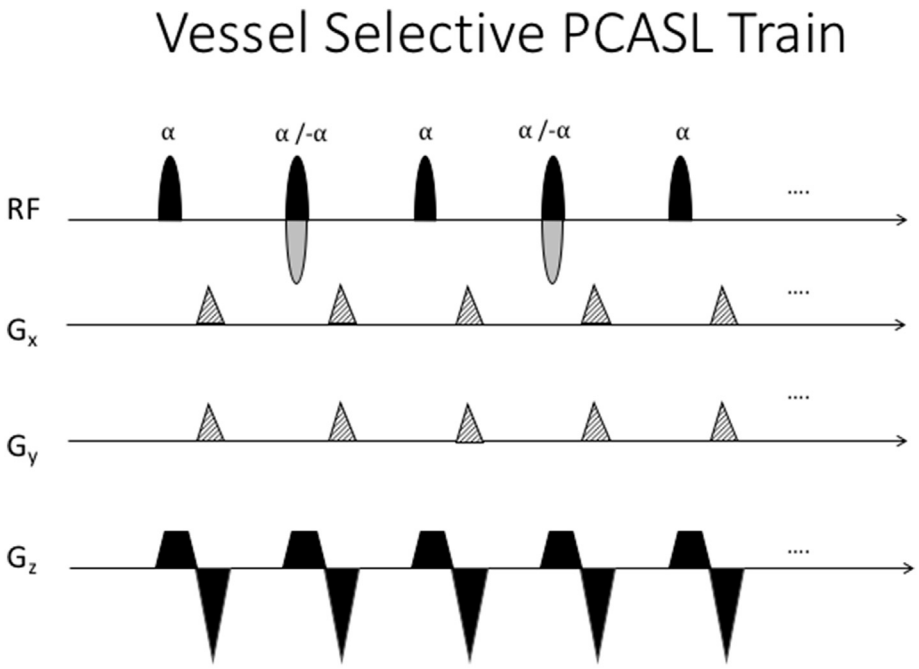

Fig. 5. A vessel selective pseudo-continuous labeling pulse train. G_x and G_y represent the additional in-plane gradients which allow to label individual vessels within the labeling plane. These gradients are played in the gap between RF pulses, typically at the same time as the rephaser of the slice selective gradient. In the control case, the sign of the RF pulses is alternated every other pulse (shown in grey).

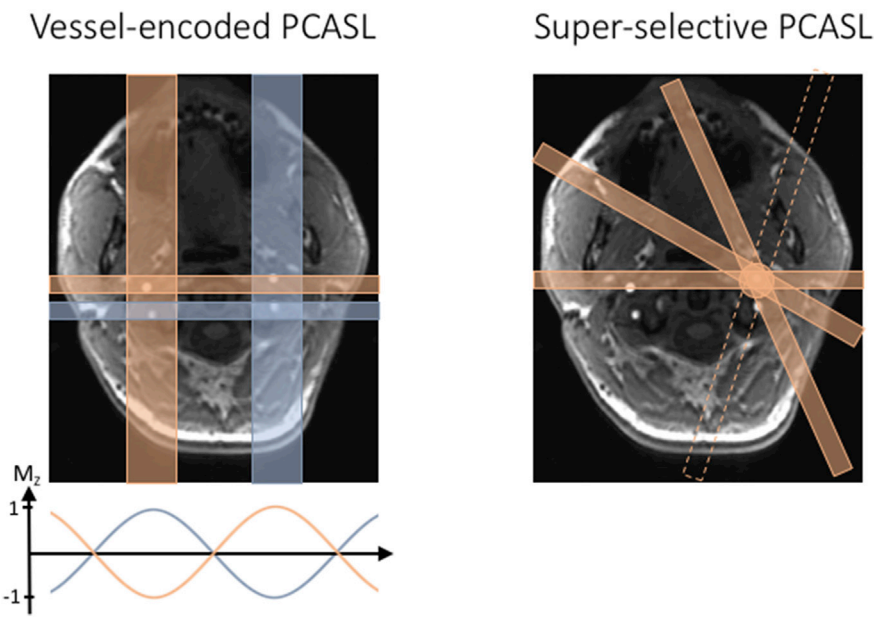

Fig. 6. Vessel-selective labeling schemes. The left panel shows a vessel-encoded labeling pattern that labels specific groups of arteries. The in-plane gradients generate a linear phase variation along the gradient direction, resulting in an approximately sinusoidal inversion profile across the label plane. The individual perfusion territories are then calculated by either solving a set of linear equations or by using a clustering approach. The right panel shows a schematic of the super-selective labeling scheme, which can isolate individual arteries by rotating the "labeling band" during the pseudo continuous labeling train of pulses.

images by inverting the Hadamard encoding matrix.

In order to avoid time-consuming calibration of the labeling scheme to the subject's anatomy and to facilitate clinical use, a "planning-free" application of ve-pcasl has gained popularity. Based on a population-averaged vessel anatomy, a standardized set of vessel-encoding steps can be derived. Instead of carefully placing the label and control stripes on the target vessels, a fixed gradient amplitude and orientation, as well as phase shift is assumed for all subjects. Subsequently, the individual vessels' contribution to each voxel is calculated by a clustering algorithm (Gevers et al., 2012). Most commonly used, the κ-mean clustering algorithm partitions the acquired perfusion maps into multiple territories by grouping voxels with similar inversion properties over all the vessel encoded images. This clustering approach works for any number of encoding steps. Identifying the individual contributions from multiple vessels in regions that are perfused by multiple sources is challenging. In order to identify the contributions of individual vessels to mixed perfusion areas (e.g. watershed region), the κ-mean clustering can be supplemented with a linear analysis or be replaced by a Bayesian interference framework (Chappell et al., 2010; Hartkamp et al., 2014).

Ve-pcasl has also been adopted to quantify territorial perfusion in the absence of anatomical information (location of vessels within labeling plane). "Blind detection" of vessel location as well as territorial perfusion can be achieved by applying a large set encoding steps with random orientation and spacing (Wong and Guo, 2012) or by using a Bayesian interference framework (Chappell et al., 2010). More recent work has focused on optimizing ve-pcasl in terms of SNR and scanning time. Berry et al. (2015) proposed a framework to estimate SNR-optimized encoding steps based on Fourier Transformation which works for any number and assembly of vessels. A fast planning-free ve-pcasl approach was introduced by Zhang et al. (2016), which has shown to reduce the total acquisition time by interleaving blocks of label and control for different encoding steps.

As an alternative to ve-pcasl, Helle et al. (2010) and Dai et al. (2010) introduced the concept of super-selective pcasl to allow for the labeling of a single vessel. In this approach, the in-plane gradients are rotated within the label plane after each RF pulse, thereby creating a circular labeling area which can be placed freely on vessels in the neck and cranium (See the right panel of Fig. 6). By changing the amplitude of the transverse gradients, the size of the label spot can be adjusted, providing precise measurements of individual perfusion territories. In comparison to ve-pcasl, super-selective PCASL does not require complicated post-processing to identify perfusion from an individual vessel. However, super-selective pcasl requires careful positioning of the label spot based on the subject's anatomy.

Modeling the ASL signal

The ability to quantify physiological parameters, perfusion in particular, has motivated much of the development of ASL techniques. In the ASL literature, the single compartment model introduced by Buxton et al. (1998) has generally been the *de facto* standard, and its solution for the continuous labeling case with post labeling delays is the recommended consensus implementation (Alsop et al., 2015) for routine use (The only difference between the two is that the former assumes that blood relaxes with the T1 of tissue when it enters the voxels, while the latter assumes that it continues to relax at the same rate as in the arteries). This model captures the behavior of the ASL signal in ideal continuous labeling experiments. However, it is also accepted that the behavior of the ASL signal is a bit more complex than that, and more complete models have also been proposed in order to capture the signal behavior (Parkes, 2005; Zhou et al., 2001). Other types of ASL acquisitions, such as Look-Locker (Brookes et al., 2007; Capron et al., 2013; Noguchi et al., 2012) or fingerprinting acquisitions (Su et al., 2016; Wright, 2014) have also used modified versions of the model to account for these advanced acquisition techniques. As we will soon discuss, research has been focused on one and two compartment models, as well as the label dispersion in the arteries while in transit (Chappell et al., 2013). Additional factors like the permeability of the vessels has also been explored (Ewing et al., 2006; St. Lawrence et al., 2012; Wang et al., 2007).

Originally, the ASL signal was modeled by modification of the Bloch equations to include the inflow and outflow of blood magnetization (Detre et al., 1992; Williams et al., 1992). In the single compartmental model, it is assumed that blood enters the voxel volume being imaged through an artery and the exchange of water from the artery to the tissue is comprehensive and instantaneous, i.e., assuming a well-mixed compartment at the imaging voxel.

Another (simpler and more popular) way of describing the ASL signal in a single compartment model is through the convolution of the arterial magnetization function with a product of the "residue" (also referred to as "retention") function $r(t)$, and a magnetization relaxation function $m(t)$ (Buxton et al., 1998; Wong et al., 1998).

The principal problem in using a single compartment model to describe the ASL signal is that the well-mixed compartment assumption does not hold very well in practice (see Fig. 8). The underlying assumption of instantaneous exchange of vascular water with tissue implies that water in the voxel will relax with the $T1$ of tissue during the entirety of the ASL experiment, when in fact a portion of the blood relaxes with the $T1$ of blood before entering the tissue itself. This results in lower overall relaxation rates of labeled water in reality, because the $T1$ of water in blood is longer than $T1$ of water in tissue. Another aspect that leads to error is the assumption that all the blood in the artery is exchanged with the tissue in the voxel, whereas actually, a portion of the arriving blood passes through the voxel without exchanging water with the tissue.

The two-compartment model (see Fig. 7) corrects for these effects by introduction of an additional compartment inside the voxel, where the blood enters from the artery. Exchange of water form this blood compartment into the tissue compartment occurs through the membrane separating the tissue and blood compartment, which is considered to be semipermeable. When this exchange is allowed, it is expressed with the help of the permeability-surface area (PS) product (Parkes, 2005; Ewing et al., 2001; St. Lawrence et al., 2012; Wang et al., 2007). When the assumption is that there is no exchange of labeled water between the blood and the tissue compartment, the permeability surface area product becomes unnecessary. Instead, it is assumed that the arterial input to the voxel branches into two components, a component that feeds blood into the tissue compartment and is absorbed in entirety, and a non-permeable pass-through arterial component, where there is no interaction with the tissue compartment.

In recent work for the purposes of ASL fingerprinting, Su et al. modified the Bloch equations for the two-compartmental model (see Fig. 7) in order to capture the effects of arterial water flowing through a voxel without exchanging into the extravascular space (Su et al., 2016).

There has been a significant effort to include the effects of the dispersion of the blood particles as they travel from the labeling location to the imaging voxel. The arterial input function (AIF) describes the concentration of the label arriving at the tissue voxel as a function of time. The ideal AIF for CASL would be a delayed box car shape reflecting the labeling scheme- indicating that the labeled bolus arrives at the imaging voxel identically to the manner in which it was labeled in the labeling plane. Early ASL work only accounted for the T1 relaxation of the arterial label and the transit time of the label from the labeling plane to the imaging slice (also referred to as "bolus arrival time"). However, such a formulation is inaccurate because in reality, deviations from the ideal situation above arise due to the labeled spins arriving at the imaging voxel at different speeds. In early work, Hrabe and Lewis (2004) included a Gaussian shaped dispersion kernel to capture this effect. Gallichan et al. introduced another dispersion model capturing the effects of laminar flow velocity profiles into the arrival time (Gallichan and Jezzard, 2008). However, more recent work from Chappell et al. demonstrated that a Gamma-Variate function was a better fit to the dispersion observed in the arterial input function (Chappell et al., 2013).

Physiological noise correction

The SNR of ASL images is intrinsically low, and a major contributor to the noise in ASL is signal fluctuations arising from cardiac pulsation and respiratory movements. Some recent improvements in SNR and stability of the ASL signal have been achieved by correcting the ASL time series for physiological noise. Methods used for physiological noise correction in ASL are often extended from those used in other fMRI methods. One such

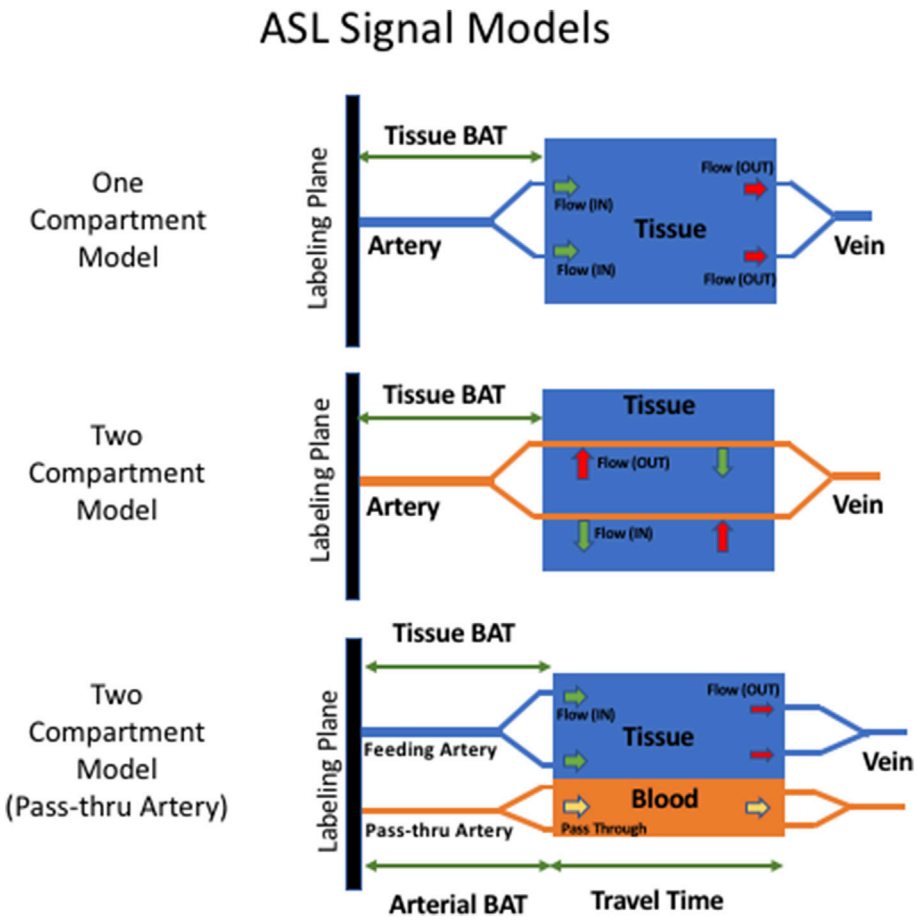

Fig. 7. The ASL signal can be modeled by describing the concentration of label in the voxel using one compartment and two compartments. The two-compartment model has also been modified in order to capture flow-thru effects.

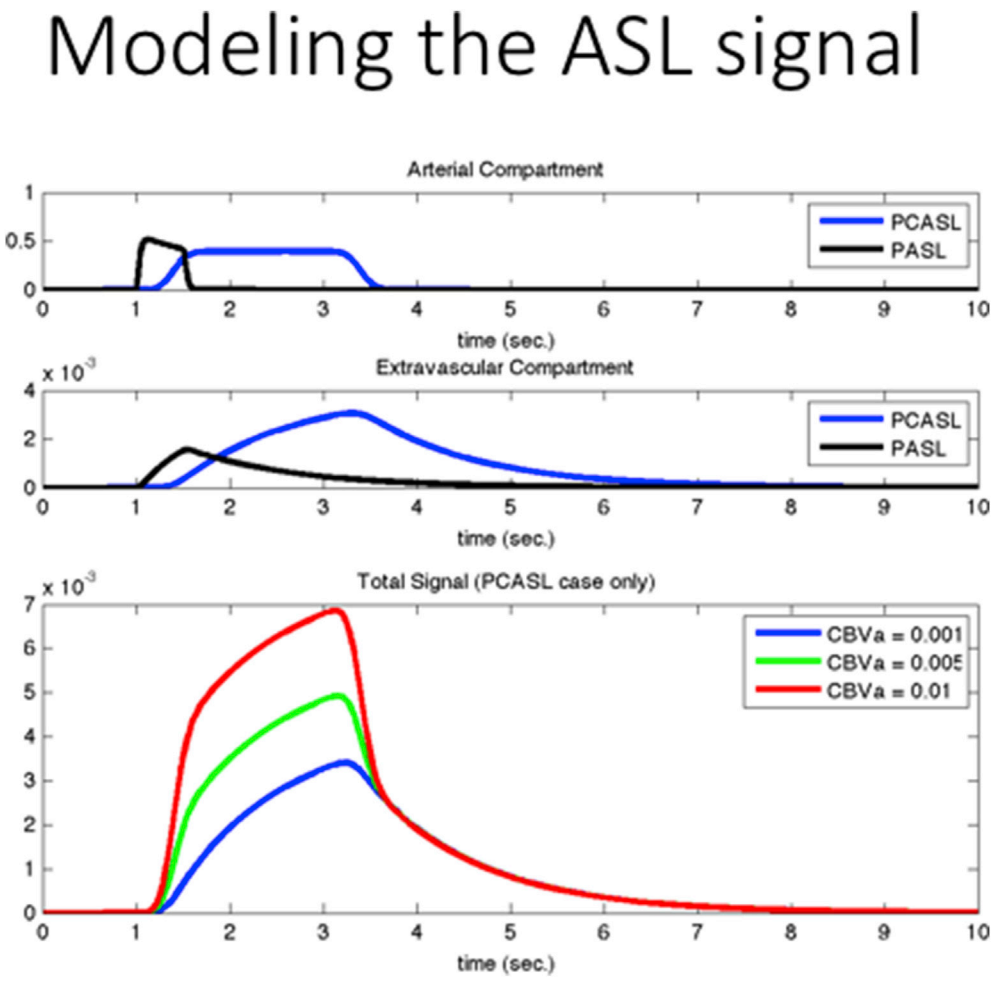

Fig. 8. ASL signal models capture the concentration of the label in a voxel as they move through the arterial compartment into the extravascular compartment, using the two-compartment model (without the pass-thru artery) in the middle panel of Fig. 7. Generally, the observed signal is the sum of the two compartments, unless the arterial compartment is suppressed during the acquisition.

popular method is RETROICOR (Glover et al., 2000) which uses low-order Fourier series to model the physiological noise component. This approach requires measurement of the physiological signals externally and removing them from an image time series through linear regression. This method was extended for ASL by Restom et al. (2006). The efficacy of the noise correction using this process depends on certain assumptions made in the modeling the noise, particularly regarding how the noise affects the control image compared to the tag image.

The CompCor method improves upon the RETROICOR procedure in that it does not require external recording (Behzadi et al., 2007). This approach uses anatomical data in combination with variance maps of the ASL time course to identify white matter and cerebrospinal fluid. Oscillations in the perfusion signal of those regions are assumed to be dominated by physiological noise, rather than neuronal activation, which is assumed to be confined to the grey matter. Then a Principal Component Analysis (PCA) from time series extracted from the white matter and the CSF regions yields time course fluctuations due to cardiac and respiratory fluctuations. The largest components can be regressed from the ASL time course, or used in tandem with a general linear model as nuisance variables.

Partial Volume Correction

Partial Volume Effects in ASL arise due to the limited resolution of the acquired images. Usually, every voxel being imaged is a combination of white matter, grey matter and cerebrospinal fluid and, as a result, the effective ASL signal is a weighted average of signals from the different components in the voxel. Another cause of partial volume effects is that MRI acquisition schemes have an inherent point spread function that translates into a blurring in the image. Due to partial volume effects, the value of flow is often underestimated, in addition to blurring the boundaries between tissue types. In order to alleviate these problems, several Partial Volume Correction (PVC) techniques have been developed.

One of the most prominent PVC techniques is the use of a linear regression method (Bruening et al., 2015) This technique involves estimating the unknown components in the expression for fractional ASL signal change:

$$\frac{\Delta M}{M_C} = \frac{(P_{GM}\Delta M_{GM}) + (P_{WM}\Delta M_{WM})}{(P_{GM}M_{GM}) + (P_{WM}M_{WM}) + (P_{CSF}M_{CSF})} \quad (2)$$

namely ΔM_i - the difference between the control and label magnetization, with i denoting the tissue type, (*GM* for grey matter, *WM* for white matter, and *CSF* for cerebrospinal fluid) and M_i – the control magnetization for tissue type i. Other known factors are the prior probabilities for tissue type i in the imaging voxel, given by P_i , and the measured control magnetization, given by M_C. The estimation is done under the assumption that the perfusion level, and therefore the ASL signal, are constant over a small region (usually a 3×3 or 5×5 kernel) around the imaging voxel. Thus, one can construct a set of overdetermined linear equations for the signals in this region, and then solve for the unknown parameters using linear regression. However, this assumption of constancy causes an inherent blurring of the images corrected through this method. Attempts at removing this effect of blurring or overall smoothing have been made (Liang et al., 2013) using modified least trimmed squares by removing outliers (in terms of residuals with respect to the kernel's central voxel) in

the regression analysis of a region.

Another prominent method for PVC is the "Bayesian Inference for Arterial Spin Labelling" (BASIL) (Chappell et al., 2009) method. This iterative method computes corrected perfusion values with a probabilistic non-linear least squares approach. Briefly, a Bayesian inference framework is used to calculate the posterior probability of the quantified parameters given the data, with the help of a likelihood term and an adaptive spatial smoothness prior for perfusion. More details about this are available to the reader in Chappell et al. (2009, 2011).

The necessary tissue type probability maps can be extracted from T1 weighted images and canonical templates. However, other methods like (Petr et al., 2013) aim at improving PVC by providing more consistent tissue probability maps (in terms of distortion and PSF) by using Look-Locker EPI for the generation of these maps, instead of using segmented high-resolution T1-weighted images. Bruening et al. also presented an improved PVC method which uses high-dimensional structural space information (thereby extending the kernel into three dimensions) to combat the effects of signal mixing due to the composition of the voxel (Bruening et al., 2015).

Beyond perfusion: ASL and other physiological parameters

Among the most exciting new applications of ASL based techniques, their application to measure additional physiological parameters beyond perfusion, sometimes by modifications to the ASL acquisition scheme, sometimes by coupling the ASL measurement with other schemes.

By simply adapting the timing of the labeling scheme, for example, one can obtain quantitative images of the arterial blood volume. This is the case of the AVAST (Arterial Volume by Arterial Spin Tagging) technique (Jahanian et al., 2015) in which the labeling time of a continuous labeling experiment is chosen to approximately match the bolus arrival time of the blood (i.e., the time it takes for the labeled spins to reach the voxel's tissue after they are labeled). Since the labeled spins have not entered the tissue yet, the observed ASL signal (i.e., subtraction of the control and labeled images) is dominated by the arterial blood, which yields an arterial blood volume weighted image. Further, if the sequence TR is reduced to match the bolus arrival time, which requires a small reduction in labeling time, then the label concentration in the extravascular space in both the control and labeled images is the same. In that case, the extravascular contribution to the ASL signal is removed by the pairwise subtraction process and the resulting image reflects only the arterial blood volume, without contamination by perfusion. Arterial blood volume is very sensitive to neuronal activation and can yield very high contrast to noise ratios in FMRI, as much of the BOLD effect is controlled by arterial vasodilation in the order to 30% (Vazquez et al., 2006; Vazquez et al., 2010).

The VASO (VAscular Space Occupancy) technique also yields blood volume measurements by nulling out the contribution of the blood through the use of inversion pulses – much like the FLAIR technique. In its original implementation, it required the injection of a contrast agent like Gd-DTPA, which does not cross the blood brain barrier (Lu et al., 2005). In latter development, this need was overcome by the iVASO technique (Inflow-Based Vascular Space Occupancy), which uses combinations of selective and non-selective labeling pulses, much like pulsed ASL techniques (Hua et al., 2011). Further progress along those lines has been made by combining labeling pulses with the sensitivity of multi-phase SSFP to inflowing blood. This technique results in high SNR, quantitative images of arterial blood volume, and could also be adapted to FMRI experiments (Yan et al., 2012).

Given that arterial spin labeling techniques can be used to isolate the blood's MR signal and that T_2 and T_2* relaxation rates are sensitive to the blood's oxygenation level, techniques like TRUST (T2-Relaxation-Under-Spin-Tagging), can yield blood oxygenation (Y_v). In a nutshell, TRUST collects several ASL images with different effective echo time, and uses those to calculate the T_2 relaxation time of the ASL subtraction signal, as depicted in Fig. 9 (Liu et al., 2016; Lu and Ge, 2008; Lu et al., 2008; Xu et al., 2009). This technique has some interesting features. The first one is that, in order to isolate the venous blood, the labeling pulse consists of a single, slab-selective, inversion pulse, applied downstream from the imaging slice (not upstream, as the regular ASL experiments), such that the returning venous blood carries the label. The second interesting feature is that the T2 weighting of the signal is generated by a T2 preparation pulse train applied immediately before the image acquisition. This train of pulses consists of a 90° pulse followed by a train of 180° pulses that flip the magnetization in the transverse plane multiple times, while T2 contrast develops, and finally a −90° pulse to return the magnetization to the z-axis. The signs of the 180° pulses follows an MLEV pattern, in order to compensate for imperfections of the B1 field (Coolen et al., 2014). The T2 weighted images of the venous blood can then be used to compute the T2 relaxation rate. Finally, T2 can be readily translated into oxygenation level by previous T2-oxygenation calibration data obtained in vitro.

The QUIXOTIC technique yields similar information by isolating the post capillary venous blood through a clever combination of velocity selective saturation pulses and blood nulling inversion pulses. It offers the ability to collect venous blood oxygenation maps in grey matter regions (not just in the major venous watersheds). In the proposed implementation, the authors demonstrated that one can use this information in conjunction with ASL perfusion maps in order to calculate maps of the oxygen extraction fraction (OEF) and the metabolic rate of oxygen in the brain (CMRO2) in addition to the venous oxygenation (Bolar et al., 2011).

Another interesting physiological parameter that can be estimated

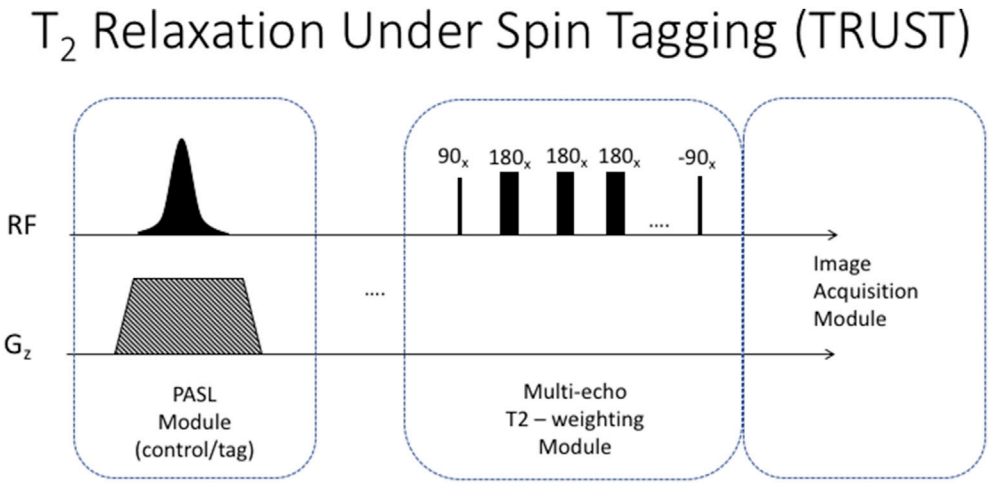

Fig. 9. The TRUST pulse sequence consists of a labeling module to isolate the venous inflow, followed by a T2 weighting module to differentiate between oxygenated and deoxygenated blood.

with the help of arterial spin labeling is arterial transit time (ATT) or Bolus Arrival Time (BAT). BAT characterizes the time it takes the labeled blood to travel from the label plane in the neck to the tissue voxel in the brain (see Figs. 7 and 8).

It has been shown that BAT can vary significantly across different regions of the brain. One source of BAT variation is the difference in velocity between feeding arteries. For example, the velocity in the vertebral arteries is generally lower than in the carotid arteries. Another cause of transit delay is a longer travel distance, which for example occurs in the presence of collateral pathways. These non-uniformities in label transport can lead to significant errors in the quantification of perfusion signal. Commonly used quantification models (section: Single compartment and two compartment models) rely on a constant BAT across brain tissue. In order to make the quantification less sensitive to differences in BAT, typically a long post-labeling delay (PLD) is chosen ($PLD >> BAT_{max}$) to guarantee that the label made it into the tissue and eliminate the contribution from the arterial compartment (Alsop and Detre, 1996). However, a long PLD leads to more label decay and therefore less SNR.

Variations in BAT are further amplified in the presence of disease. ASL perfusion images of patients with cerebrovascular disease often reveal regions of hypoperfusion. However, it is difficult to assess whether a decrease in label signal in a brain region is caused by a reduction in flow to this region or by a longer transit time. Prolonged BAT can therefore result in an underestimation of perfusion. BAT maps provide supplementary clinical information, which helps to interpret perfusion images and identify collateral pathways.

In order to acquire BAT maps, typically multiple ASL perfusion images are acquired, each with a different PLD. By tracking the perfusion signal over time, we can measure the label uptake curve on a voxel-by-voxel basis. Based on the reconstructed label uptake curve, BAT can be estimated by finding the steepest rise in label uptake (Teeuwisse et al., 2014). However, this approach can lead to errors in the case of low temporal resolution or increased noise in the images. As an alternative, a single compartment model can be fitted to the uptake curve. Typically, 5–7 PLDs are necessary to reconstruct the label uptake curve sufficiently. The most straightforward approach is to acquire images with multiple PLDs consecutively. Assuming that a single ASL image acquisition takes about 3min, this would result in a total acquisition time of approximately 15–20 min, making it unfeasible for clinical use. Hence, research in this field has primarily focused on developing more efficient schemes to increase the acquisition speed.

One example is the application of a look-locker (LL) scheme, which has shown to increase the temporal resolution of multi-PLD acquisition (Chen et al., 2012). The LL scheme is based on multiple image acquisitions, immediately following the label pulse (Fig. 10). Since each acquisition represents an increasing PLD, the gap before the next labeling period (TR) can be used efficiently. However, the LL scheme requires a low flip angle in order to acquire multiple images. While this improves the temporal resolution of the measurement, it results in a lower SNR compared to standard (single) acquisition schemes. This is especially true for the later portion of the curve, since the label will already have experienced multiple readout pulses.

As an alternative, time-encoded pcasl (te-pcasl) has been introduced to overcome low SNR and to acquire multiple PLDs in a single scan (Dai et al., 2013; Teeuwisse et al., 2014; Wells et al., 2010). Based on a Hadamard encoding scheme, te-pcasl splits up the pulse train in small blocks of labeling and control pulses (see Fig. 11). In a post-processing step, the resulting perfusion image for a specific PLD can be calculated through a combination of all image acquisitions so that only one PLD remains whereas contributions from all other PLDs cancel out. In the example shown in Fig. 11, the subtraction image for PLD 3 can be calculated as following:

$$\Delta M_{PLD3} = Image\ 1 - Image\ 2 + Image\ 3 - Image\ 4 - Image\ 5 + Image\ 6 - Image\ 7 + Image\ 8 \quad [3]$$

This approach has two major advantages. First, the combination of all acquisitions results in images with a high number of averages, which increases the SNR. Second, by using the entire time gap between the start of the pulse train and the image acquisition for blocks of label and control pulses, the entire scan can be performed in a fraction of the original scanning time for a sequential acquisition of PLDs. However, this approach also has a downside. The occurrence of artefacts, such as motion, will be carried through all images since each image is a combination of all acquisitions. More recently, It has been shown that the sensitivity to motion artefacts of te-pcasl can be reduced by replacing the Hadamard matrix with a Welsh-ordered Hadamard matrix (von Samson-Himmelstjerna et al., 2016) or by using a Bayesian decoding scheme (von Samson-Himmelstjerna et al., 2015).

ASL fingerprinting

Magnetic Resonance Fingerprinting (MRF), originally proposed as a quantitative relaxometry method robust to artefacts (Ma et al., 2013) has been recently proposed as an alternative for estimating multiple physiological parameters related to blood flow and perfusion in the brain from a single time series (Su et al., 2016; Wright, 2014). Traditionally, acquiring these additional parameters typically requires extra scans, which renders the entire process time consuming and makes it clinically impractical. MRF tries to overcome this issue by matching an observed time-series of images to a dictionary composed of unique ASL signals. Their uniqueness is ensured by a (pseudo-) randomization of the acquisition parameters, e.g., label duration, TR, post labeling delay … etc. The dictionary is generated by a signal model with multiple combinations of tissue parameters as its input, e.g., perfusion, blood volume, T1 … etc. For each combination, a modified Bloch-equation simulation is performed based on a one- or two-compartment model (as described above),

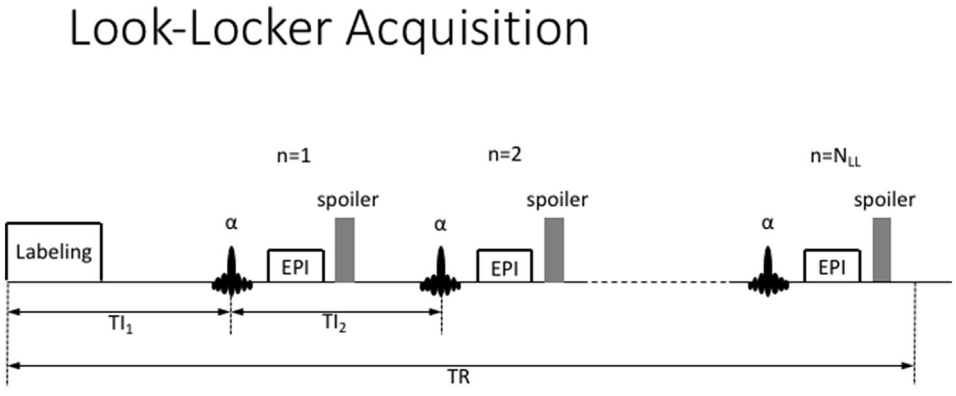

Fig. 10. A Look-Locker ASL acquisition consisting of a labeling module immediately followed by a train of fast acquisitions to capture the inflow of the label into the arterial tree and its uptake by the extra vascular compartment.

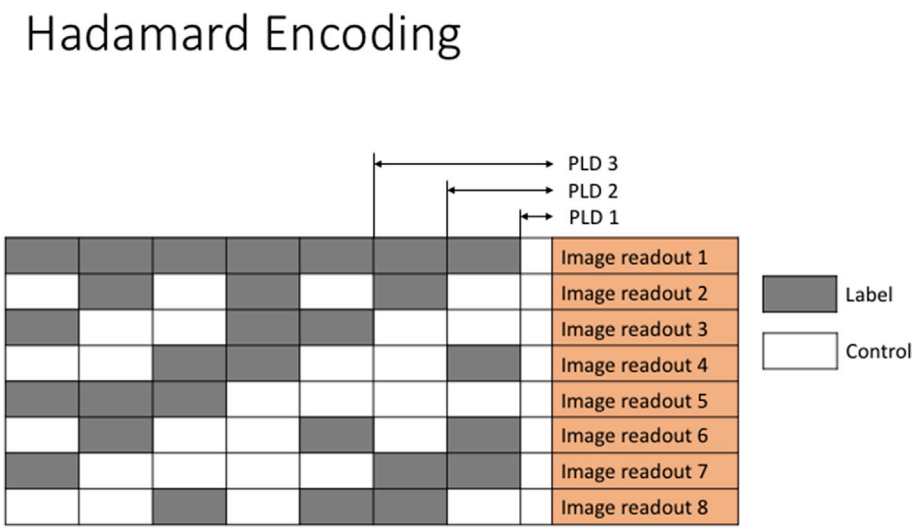

Fig. 11. Bolus Arrival Time (Arterial Transit Time) information can be obtained by multiple ASL acquisitions with varying duration and delay of the labeling function. The Hadamard encoding sequence constitutes an efficient combination of timings in order to collect the ASL input function.

and the resultant time-series (see Fig. 12) creates a single entry in the dictionary. The final step is to match each voxel's time series to the closest entry in the dictionary. The process of matching essentially mimics a Maximum Likelihood approach to estimate a set of parameters given an observation. Once the match is found, the tissue parameters used to generate the best match in the dictionary are assigned to that voxel. This process is repeated over all voxels in the imaging volume to obtain relevant parameter maps of the brain. As a result, fingerprinting can bypass difficulties in estimation caused by presence of artefacts, such as noise, off-resonance, movement or even undersampling.

ASL fingerprinting is still an active area of development. Current challenges include excessive amounts of storage space for the dictionary, as well as unacceptably long computational time to generate dictionaries and search for the best match. Despite this computational inefficiency, development of fingerprinting methods is exciting because they can be potentially robust to artefacts, while yielding multiple quantitative measurements from a single scan.

Resting state functional connectivity

Collecting a BOLD weighted time series without a specific activation paradigm or model is well known to reveal correlations in the activity among different brain areas (resting state functional connectivity rfcMRI). The spontaneous, correlated fluctuations used to identify networks using rsfcMRI are typically slow, in the range below 0.1 Hz (Biswal et al., 1997; Greicius et al., 2003). As can be expected, these fluctuations are also reflected in perfusion and several groups have demonstrated that ASL sequences can capture them and also reveal functionally connected networks similar to the ones found in BOLD imaging. Global correlations must be taken into account, as the observed ASL signal in the whole brain will fluctuate with respiration, cardiac pulsatility and any fluctuations in labeling efficiency. Despite these challenges, ASL still reveals functional networks, as first shown by Biswal et al. (1997) and further explored by others (Chuang et al., 2008; De Luca et al., 2006). BOLD weighted rsfcMRI is more sensitive, offers higher temporal resolution and is simpler to implement, but ASL offers quantification as a very attractive feature. While it is more common to perform separate ASL and BOLD connectivity scans, examples of ASL based rsfcMRI include work by Loggia et al. (2013), who examined changes in the default network related to chronic clinical pain. As the field of functional neuroimaging becomes increasingly quantitative, we can expect to see a rising trend in the use of ASL based functional connectivity imaging. An ambitious approach is to conduct interleaved ASL and BOLD time series measurements as the technique proposed by Schmithorst et al. (2014). However, the more prevalent trend is to carry out BOLD weighted rsfcFMRI studies accompanied by ASL measurements of resting perfusion as a measure of baseline activity or to account for the vascular effects of drugs, as in the case of the study by Li and Zhang (2017).

Applications

Over the first ten years since the publication of the first seminal papers, most of the research was focused on technical development, and the technique was not widely embraced by the larger imaging community. Many variants of the technique were developed trying to overcome serious challenges in SNR and resolution. For a long time, there was no clear standard implementation and it was rarely available from MRI vendors. ASL seemed like a “promising technique” under development, but only a few sites had the technical capability to use ASL in the clinic or as a research tool to investigate biological questions. In the last five to ten years, however, with the advent of improved labeling schemes, fast parallel imaging, background suppression and denoising techniques, ASL is rapidly gaining popularity in the clinic and in biomedical research. Most MRI vendor now have a standard implementation of the PCASL technique available for the new generation scanners.

Perfusion of blood through an organ is a powerful biomarker of its health and activity. As one could expect, the ability to image perfusion (dynamically, if necessary) without tracers or other invasive techniques has found many applications. In this section, we would like to survey a few recent applications of ASL, to illustrate the potential uses of the ASL technique, paying particular attention to neuroimaging applications.

To begin, much of the development of ASL techniques has been motivated by neurodegenerative and stroke research. Some of the earliest applications were centered on vascular disease, particularly stroke (Bokkers et al., 2012; Chalela et al., 2000; Wang et al., 2012; Zaharchuk et al., 2012). For a thorough review of clinical neuroimaging applications of ASL, please see (Haller et al., 2016). More recently, the connection between vascular health and neurodegenerative disorders has become increasingly clear and has motivated many perfusion imaging studies in Alzheimer's (Alsop et al., 2000; Benedictus et al., 2016; De La Torre, 2004; Iadecola, 2004; Iturria-Medina et al., 2016) and Parkinson's (Fernandez-Seara et al., 2012) diseases. In the case of Alzheimer's disease, COST (the European Cooperation in Science and Technology) has been pursuing and funding an initiative to develop ASL as a tool to investigate and diagnose Alzheimers and other forms of dementia (http://aslindementia.org).

In this regard cognitive decline is strongly associated with hypoperfusion, which can also be a predictor of conversion from mild cognitive impairment to full blown dementia (Chao et al., 2010; Wierenga et al., 2014). Recent studies have shown that perfusion imaging can

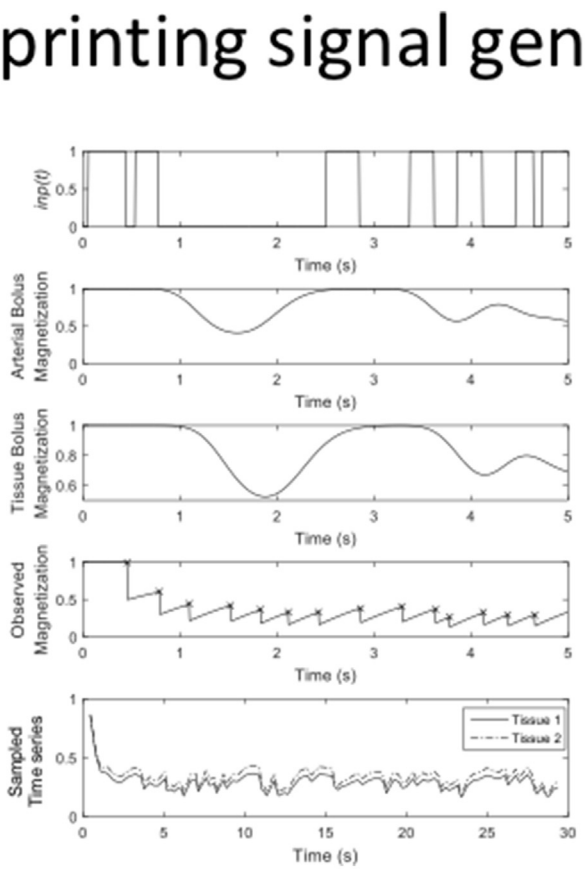

Fig. 12. ASL fingerprinting. A pseudo-random labeling scheme is used to generate an image time series whose signal is unique for a given combination of hemodynamic parameters. The top panel indicates a labeling function, the second panel shows the concentration of the label in the arterial compartment. Similarly, the third panel shows the concentration of the label in the extra-vascular compartment. The total magnetization (spin history) of the whole voxel is plotted in the fourth compartment. Finally, the bottom panel shows the observed time series from two different voxels.

also be informative about the severity of Parkinson's disease and it can also yield insights about its etiology and mechanism (Lin et al., 2017; Syrimi et al., 2017; Yamashita et al., 2017).

Perfusion imaging can be a key tool to examine longitudinal changes in brain function following an intervention, such as transcranial magnetic stimulation, cognitive training, or pharmacological treatment, in part because of their statistical properties (Aguirre et al., 2002). ASL techniques are largely immune to scanner drifts and can be used to quantify physiological parameters. For example, a recent study by Buch et al. (2016) on caffeine and acetazolamide challenges (well known vasoactive drugs) highlights the utility of ASL techniques to probe changes in brain function caused by pharmacological intervention within a scanning session. At the same time, ASL based FMRI experiments can yield insights on the effects of psychoactive drugs over the course of the treatment, as in the recent study by Liemburg et al. (2017), which showed differential effects between two different schizophrenia treatment medications in terms of how these affected the brain's response to emotional stimuli. ASL has also been used to identify the networks affected by Gamma hydroxybutarate (GHB) in a double-blind, randomized cross-over design trial (Bosch et al., 2017). As another example, a randomized, double-blind, crossover phase II study is underway to examine the use of Tadalafil as a treatment for small vessel disease (SVD) and vascular cognitive impairment (VCI) (Pauls et al., 2017).

One of the dominant application of ASL is in cognitive psychology research. Notably, a recent large study of older participants (>70 years old) showed a clear correlation between several measures of cognition and baseline CBF (Hshieh et al., 2017). As an example of a task based ASL FMRI study, Buschkuel et al. investigated the effect of working memory training on brain function during an N-back task. In their study, they showed that the improvement in performance was accompanied by perfusion differences in the brain both at rest and during task performance in selected regions (Buschkuehl et al., 2014).

Finally, although the focus of this article is primarily brain imaging, it should also be noted that ASL is being used for other organs with increasing frequency, particularly the kidney (Duhamel et al., 2014; Mora-Gutierrez et al., 2017; Zimmer et al., 2013). A recent validation was carried out recently comparing ASL to dynamic contrast enhancement methods in the kidney by Conlin et al. (2017).

References

Aguirre, G.K., Detre, J. a, Zarahn, E., Alsop, D.C., 2002. Experimental design and the relative sensitivity of BOLD and perfusion fMRI. NeuroImage 15 (3), 488–500. http://doi.org/10.1006/nimg.2001.0990.

Alsop, D.C., Detre, J. a, 1996. Reduced transit-time sensitivity in noninvasive magnetic resonance imaging of human cerebral blood flow. J. Cerebr. Blood Flow Metabol. 16 (6), 1236–1249. http://doi.org/10.1097/00004647-199611000-00019.

Alsop, D.C., Detre, J.A., Golay, X., Günther, M., Hendrikse, J., Hernandez-Garcia, L., et al., 2015. Recommended implementation of arterial spin-labeled Perfusion mri for clinical applications: a consensus of the ISMRM Perfusion Study group and the European consortium for ASL in dementia. Magn. Reson. Med. 73 (1). http://doi.org/10.1002/mrm.25197.

Alsop, D.C., Detre, J. a, Grossman, M., 2000. Assessment of cerebral blood flow in Alzheimer's disease by spin-labeled magnetic resonance imaging. Ann. Neurol. 47 (1), 93–100. http://doi.org/https://doi.org/10.1002/1531-8249%28200001%2947:1%3C93::AID-ANA15%3E3.0.CO;2-8.

Behzadi, Y., Restom, K., Liau, J., Liu, T.T., 2007. A component based noise correction method (CompCor) for BOLD and perfusion based fMRI. NeuroImage 37 (1), 90–101. http://doi.org/10.1016/j.neuroimage.2007.04.042.

Benedictus, M.R., Leeuwis, A.E., Binnewijzend, M.A.A., Kuijer, J.P.A., Scheltens, P., Barkhof, F., et al., 2016. Lower cerebral blood flow is associated with faster cognitive decline in Alzheimer's disease. Eur. Radiol. 27 (3), 1–7. http://doi.org/10.1007/s00330-016-4450-z.

Berry, E.S.K., Jezzard, P., Okell, T.W., 2015. An optimized encoding scheme for planning vessel-encoded pseudocontinuous arterial spin labeling. Magn. Reson. Med. 74 (5), 1248–1256. http://doi.org/10.1002/mrm.25508.

Biswal, B.B., Kylen, J. Van, Hyde, J.S., 1997. Simultaneous assessment of flow and BOLD signals in resting-state functional connectivity maps. NMR Biomed. 10 (45), 165–170.

Blaimer, M., Breuer, F., Mueller, M., Heidemann, R.M., Griswold, M. a, Jakob, P.M., 2004. SMASH, SENSE, PILS, GRAPPA: how to choose the optimal method. Top. Magn. Reson. Imag. TMRI 15 (4), 223–236. http://doi.org/10.1097/01.rmr.0000136558.09801.dd.

Bokkers, R.P.H., Hernandez, D.A., Merino, J.G., Mirasol, R.V., van Osch, M.J., Hendrikse, J., et al., 2012. Whole-brain arterial spin labeling perfusion MRI in patients with acute stroke. Stroke 43 (5), 1290–1294.

Bolar, D.S., Rosen, B.R., Sorensen, A.G., Adalsteinsson, E., 2011. QUantitative Imaging of eXtraction of oxygen and TIssue consumption (QUIXOTIC) using venular-targeted velocity-selective spin labeling. Magn. Reson. Med. 66 (6), 1550–1562. http://doi.org/10.1002/mrm.22946.

Bosch, O.G., Esposito, F., Havranek, M.M., Dornbierer, D., von Rotz, R., Staempfli, P., et al., 2017. Gamma-hydroxybutyrate increases resting state limbic perfusion and body and emotion awareness in humans. Neuropsychopharmacology. http://doi.org/10.1038/npp.2017.110.

Brookes, M.J., Morris, P.G., Gowland, P. a., Francis, S.T., 2007. Noninvasive measurement of arterial cerebral blood volume using Look-Locker EPI and arterial spin labeling. Magn. Reson. Med. 58 (1), 41–54. http://doi.org/10.1002/mrm.21199.

Bruening, D.E., Dharssi, S., Lazar, R.M., Marshall, R.S., Asllani, I., 2015. Improved partial volume correction method for detecting brain activation in disease using Arterial Spin Labeling (ASL) fMRI. In: 2015 37th Annual International Conference of the IEEE Engineering in Medicine and Biology Society (EMBC), C, pp. 5441–5444. http://doi.org/10.1109/EMBC.2015.7319622.

Buch, S., Ye, Y., Haacke, E.M., 2016. Quantifying the changes in oxygen extraction fraction and cerebral activity caused by caffeine and acetazolamide. J. Cerebr. Blood Flow Metabol. 0271678X16641129 http://doi.org/10.1177/0271678X16641129.

Buschkuehl, M., Hernandez-Garcia, L., Jaeggi, S.M., Bernard, J. a, Jonides, J., 2014. Neural effects of short-term training on working memory. Cognit. Affect. Behav. Neurosci. 14, 147–160. http://doi.org/10.3758/s13415-013-0244-9.

Buxton, R.B., Frank, L.R., Wong, E.C., Siewert, B., Warach, S., Edelman, R.R., 1998. A general kinetic model for quantitative perfusion imaging with arterial spin labeling. Magn. Reson. Med. Off. J. Soc. Magn. Reson. Med. 40, 383–396. http://doi.org/10.1002/mrm.1910400308.

Capron, T., Troalen, T., Cozzone, P.J., Bernard, M., Kober, F., 2013. Cine-ASL: a steady-pulsed arterial spin labeling method for myocardial perfusion mapping in mice. Part II. Theoretical model and sensitivity optimization. Magn. Reson. Med. 70 (5), 1399–1408. http://doi.org/10.1002/mrm.24588.

Chalela, J.A., Alsop, D.C., Gonzalez-Atavales, J.B., Maldjian, J.A., Kasner, S.E., Detre, J.A., 2000. Magnetic resonance perfusion imaging in acute ischemic stroke using continuous arterial spin labeling. Stroke 31 (3), 680–687. Retrieved from. http://www.ncbi.nlm.nih.gov/entrez/query.fcgi?cmd=Retrieve&db=PubMed&dopt=Citation&list_uids=10700504.

Chao, L.L., Buckley, S.T., Kornak, J., Schuff, N., Madison, C., Yaffe, K., et al., 2010. ASL perfusion MRI predicts cognitive decline and conversion from MCI to dementia. Alzheimer Dis. Assoc. Disord. 24 (1), 19.

Chappell, M.A., Groves, A.R., MacIntosh, B.J., Donahue, M.J., Jezzard, P., Woolrich, M.W., 2011. Partial volume correction of multiple inversion time arterial spin labeling MRI data. Magn. Reson. Med. 65 (4), 1173–1183. http://doi.org/10.1002/mrm.22641.

Chappell, M.A., Groves, A.R., Whitcher, B., Woolrich, M.W., 2009. Variational Bayesian inference for a nonlinear forward model. IEEE Trans. Signal Process. 57 (1), 223–236. http://doi.org/10.1109/TSP.2008.2005752.

Chappell, M.A., Okell, T.W., Jezzard, P., Woolrich, M.W., 2010. A general framework for the analysis of vessel encoded arterial spin labeling for vascular territory mapping. Magn. Reson. Med. 64 (5), 1529–1539. http://doi.org/10.1002/mrm.22524.

Chappell, M. a., Woolrich, M.W., Kazan, S., Jezzard, P., Payne, S.J., MacIntosh, B.J., 2013. Modeling dispersion in arterial spin labeling: validation using dynamic angiographic measurements. Magn. Reson. Med. 69 (2), 563–570. http://doi.org/10.1002/mrm.24260.

Chen, J.J., Wieckowska, M., Meyer, E., Pike, G.B., 2008. Cerebral blood flow measurement using fMRI and PET: a cross-validation study. Int. J. Biomed. Imag. 2008, 516359. http://doi.org/10.1155/2008/516359.

Chen, Y., Wang, D.J.J., Detre, J. a, 2011. Test-retest reliability of arterial spin labeling with common labeling strategies. J. Magn. Reson. Imag. 33 (4), 940–949. http://doi.org/10.1002/jmri.22345.

Chen, Y., Wang, D.J.J., Detre, J.A., 2012. Comparison of arterial transit times estimated using arterial spin labeling. Magn. Reson. Mater. Phys. Biol. Med. 25 (2), 135–144. http://doi.org/10.1007/s10334-011-0276-5.

Chuang, K.-H., van Gelderen, P., Merkle, H., Bodurka, J., Ikonomidou, V.N., Koretsky, A.P., et al., 2008. Mapping resting-state functional connectivity using perfusion MRI. NeuroImage 40 (4), 1595–1605. http://doi.org/10.1016/j.neuroimage.2008.01.006.

Conlin, C.C., Oesingmann, N., Bolster, B., Huang, Y., Lee, V.S., Zhang, J.L., 2017. Renal plasma flow (RPF) measured with multiple-inversion-time arterial spin labeling (ASL) and tracer kinetic analysis: validation against a dynamic contrast-enhancement method. Magn. Reson. Imag. 37, 51–55. http://doi.org/10.1016/j.mri.2016.11.010.

Coolen, B.F., Simonis, F.F.J., Geelen, T., Moonen, R.P.M., Arslan, F., Paulis, L.E.M., et al., 2014. Quantitative T2 mapping of the mouse heart by segmented MLEV phase-cycled T2 preparation. Magn. Reson. Med. 72 (2), 409–417.

Dai, W., Garcia, D., De Bazelaire, C., Alsop, D.C., 2008. Continuous flow-driven inversion for arterial spin labeling using pulsed radio frequency and gradient fields. Magn. Reson. Med. 60 (6), 1488–1497. http://doi.org/10.1002/mrm.21790.

Dai, W., Robson, P.M., Shankaranarayanan, A., Alsop, D.C., 2010. Modified pulsed continuous arterial spin labeling for labeling of a single artery. Magn. Reson. Med. 64 (4), 975–982. http://doi.org/10.1002/mrm.22363.

Dai, W., Shankaranarayanan, A., Alsop, D.C., 2013. Volumetric measurement of perfusion and arterial transit delay using hadamard encoded continuous arterial spin labeling. Magn. Reson. Med. 69 (4), 1014–1022. http://doi.org/10.1002/mrm.24335.

De La Torre, J.C., 2004. Is Alzheimer's disease a neurodegenerative or a vascular disorder? Data, dogma, and dialectics. Lancet Neurol. 3 (3), 184–190. http://doi.org/10.1016/S1474-4422(04)00683-0.

De Luca, M., Beckmann, C.F., De Stefano, N., Matthews, P.M., Smith, S.M., 2006. fMRI resting state networks define distinct modes of long-distance interactions in the human brain. NeuroImage 29 (4), 1359–1367. https://doi.org/10.1016/j.neuroimage.2005.08.035.

Deshmane, A., Gulani, V., Griswold, M.A., Seiberlich, N., 2012. Parallel MR imaging. J. Magn. Reson. Imag. 36 (1), 55–72. http://doi.org/10.1002/jmri.23639.

Detre, J. a, Leigh, J.S., Williams, D.S., Koretsky, a P., 1992. Perfusion imaging. Magn. Reson. Med. Off. J. Soc. Magn. Reson. Med. 23 (1), 37–45. http://doi.org/10.1002/mrm.1910230106.

Duhamel, G., Prevost, V., Girard, O.M., Callot, V., Cozzone, P.J., 2014. High-resolution mouse kidney perfusion imaging by pseudo-continuous arterial spin labeling at 11.75T. Magn. Reson. Med. 71, 1186–1196. http://doi.org/10.1002/mrm.24740.

Ewing, J.R., Brown, S.L., Lu, M., Panda, S., Ding, G., Knight, R. a, et al., 2006. Model selection in magnetic resonance imaging measurements of vascular permeability: Gadomer in a 9L model of rat cerebral tumor. J. Cerebr. Blood Flow Metabol. Off. J. Int. Soc. Cerebr. Blood Flow Metabol. 26 (3), 310–320. http://doi.org/10.1038/sj.jcbfm.9600189.

Ewing, J.R., Cao, Y., Fenstermacher, J., 2001. Single-coil arterial spin-tagging for estimating cerebral blood flow as viewed from the capillary: relative contributions of intra- and extravascular signal. Magn. Reson. Med. 46 (3), 465–475. http://doi.org/10.1002/mrm.1215.

Ewing, J.R., Cao, Y., Knight, R. a., Fenstermacher, J.D., 2005. Arterial spin labeling: validity testing and comparison studies. J. Magn. Reson. Imag. 22 (6), 737–740. http://doi.org/10.1002/jmri.20451.

Fernandez-Seara, M. a, Mengual, E., Vidorreta, M., Aznarez-Sanado, M., Loayza, F.R., Villagra, F., et al., 2012. Cortical hypoperfusion in Parkinson's disease assessed using arterial spin labeled perfusion MRI. Neuroimage 59 (3), 2743–2750. http://doi.org/10.1016/j.neuroimage.2011.10.033.

Gallichan, D., Jezzard, P., 2008. Modeling the effects of dispersion and pulsatility of blood flow in pulsed arterial spin labeling. Magn. Reson. Med. 60 (1), 53–63. http://doi.org/10.1002/mrm.21654.

Gao, Y., Goodnough, C.L., Erokwu, B.O., Farr, G.W., Darrah, R., Lu, L., et al., 2014. Arterial spin labeling-fast imaging with steady-state free precession (ASL-FISP): a rapid and quantitative perfusion technique for high-field MRI. NMR Biomed. 27 (8), 996–1004. http://doi.org/10.1002/nbm.3143.

Garcia, D.M., Duhamel, G., Alsop, D.C., 2005. Efficiency of inversion pulses for background suppressed arterial spin labeling. Magn. Reson. Med. 54 (2), 366–372. http://doi.org/10.1002/mrm.20556.

Gevers, S., Bokkers, R.P., Hendrikse, J., Majoie, C.B., Kies, D.A., Teeuwisse, W.M., et al., 2012. Robustness and reproducibility of flow territories defined by planning-free vessel- encoded pseudocontinuous arterial spin-labeling. Am. J. Neuroradiol. 33 (2), 21–25. http://doi.org/10.3174/ajnr.A2410.

Glover, G.A.R.Y.H., I, T.I.E.I.L., Ess, D.A.R., 2000. Image-based method for retrospective correction of physiological motion effects in fMRI. RETROICOR 167 (March), 162–167.

Greicius, M.D., Krasnow, B., Reiss, A.L., Menon, V., 2003. Functional connectivity in the resting brain: a network analysis of the default mode hypothesis. Proc. Natl. Acad. Sci. Unit. States Am. 100 (1), 253–258. http://doi.org/10.1073/pnas.0135058100.

Guo, J., Meakin, J. a., Jezzard, P., Wong, E.C., 2014. An optimized design to reduce eddy current sensitivity in velocity-selective arterial spin labeling using symmetric BIR-8 pulses. Magn. Reson. Med. n/a-n/a http://doi.org/10.1002/mrm.25227.

Haller, S., Zaharchuk, G., Thomas, D.L., Lovblad, K.-O., Barkhof, F., Golay, X., 2016. Arterial spin labeling perfusion of the brain: emerging clinical applications. Radiology 281 (2), 337–356. http://doi.org/10.1148/radiol.2016150789.

Hartkamp, N.S., Helle, M., Chappell, M.A., Okell, T.W., Hendrikse, J., Bokkers, R.P.H., Van Osch, M.J.P., 2014. Validation of planning-free vessel-encoded pseudo-continuous arterial spin labeling MR imaging as territorial-ASL strategy by comparison to super-selective p-CASL MRI. Magn. Reson. Med. 71 (6), 2059–2070. http://doi.org/10.1002/mrm.24872.

Helle, M., Norris, D.G., Rüfer, S., Alfke, K., Jansen, O., Van Osch, M.J.P., 2010. Superselective pseudocontinuous arterial spin labeling. Magn. Reson. Med. 64 (3), 777–786. http://doi.org/10.1002/mrm.22451.

Hrabe, J., Lewis, D.P., 2004. Two analytical solutions for a model of pulsed arterial spin labeling with randomized blood arrival times. J. Magn. Reson. 167 (1), 49–55. http://doi.org/10.1016/j.jmr.2003.11.002.

Hshieh, T.T., Dai, W., Cavallari, M., Guttmann, C.R., Meier, D.S., Schmitt, E.M., et al., 2017. Cerebral blood flow MRI in the nondemented elderly is not predictive of post-operative delirium but is correlated with cognitive performance. J. Cerebr. Blood Flow Metabol. 37 (4), 1386–1397. http://doi.org/10.1177/0271678X16656014.

Hua, J., Qin, Q., Donahue, M.J., Zhou, J., Pekar, J.J., Van Zijl, P.C.M., 2011. Inflow-based vascular-space-occupancy (iVASO) MRI. Magn. Reson. Med. 66 (1), 40–56. http://doi.org/10.1002/mrm.22775.

Iadecola, C., 2004. Neurovascular regulation in the normal brain and in Alzheimer's disease. Nat. Rev. Neurosci. 5 (5), 347–360. http://doi.org/10.1038/nrn1387.

Iturria-Medina, Y., Sotero, R.C., Toussaint, P.J., Mateos-Pérez, J.M., Evans, A.C., Weiner, M.W., et al., 2016. Early role of vascular dysregulation on late-onset Alzheimer's disease based on multifactorial data-driven analysis. Nat. Commun. 7 (May). http://doi.org/10.1038/ncomms11934.

Jahanian, H., Peltier, S., Noll, D.C., Garcia, L.H., 2015. Arterial cerebral blood volume-weighted functional MRI using pseudocontinuous arterial spin tagging (AVAST). Magn. Reson. Med. 73 (3). http://doi.org/10.1002/mrm.25220.

Li, C.-X., Zhang, X., 2017. Effects of long-duration administration of 1% isoflurane on resting cerebral blood flow and default mode network in macaque monkeys. Brain Connect. 7 (2), 98–105.

Liang, X., Connelly, A., Calamante, F., 2013. Improved partial volume correction for single inversion time arterial spin labeling data. Magn. Reson. Med. 69 (2), 531–537. http://doi.org/10.1002/mrm.24279.

Liemburg, E.J., van Es, F., Knegtering, H., Aleman, A., 2017. Effects of aripiprazole versus risperidone on brain activation during planning and social-emotional evaluation schizophrenia: a single-blind randomized exploratory study. Prog. Neuro Psychopharmacol. Biol. Psychiatr. 79 (Part B), 112–119.

Lin, W.-C., Chen, P.-C., Huang, C.-C., Tsai, N.-W., Chen, H.-L., Wang, H.-C., et al., 2017. Autonomic function impairment and brain perfusion deficit in Parkinson's disease. Front. Neurol. 8.

Liu, P., Dimitrov, I., Andrews, T., Crane, D.E., Dariotis, J.K., Desmond, J., et al., 2016. Multisite evaluations of a T2-relaxation-under-spin-tagging (TRUST) MRI technique to measure brain oxygenation. Magn. Reson. Med. 75 (2), 680–687. http://doi.org/10.1002/mrm.25627.

Loggia, M.L., Kim, J., Gollub, R.L., Vangel, M.G., Kirsch, I., Kong, J., et al., 2013. Default mode network connectivity encodes clinical pain: an arterial spin labeling study. Pain 154 (1), 24–33. http://doi.org/10.1016/j.pain.2012.07.029.

Lu, H., Ge, Y., 2008. Quantitative evaluation of oxygenation in venous vessels using T2-relaxation-under-spin-tagging MRI. Magn. Reson. Med. 60 (2), 357–363. http://doi.org/10.1002/mrm.21627.

Lu, H., Law, M., Johnson, G., Ge, Y., Van Zijl, P.C.M., Helpern, J. a, 2005. Novel approach to the measurement of absolute cerebral blood volume using vascular-space-occupancy magnetic resonance imaging. Magn. Reson. Med. 54 (6), 1403–1411. http://doi.org/10.1002/mrm.20705.

Lu, H., Zhao, C., Ge, Y., Lewis-Amezcua, K., 2008. Baseline blood oxygenation modulates response amplitude: physiologic basis for intersubject variations in functional MRI signals. Magn. Reson. Med. 60 (2), 364–372. http://doi.org/10.1002/mrm.21686.

Ma, D., Gulani, V., Seiberlich, N., Liu, K., Sunshine, J.L., Duerk, J.L., Griswold, M. a, 2013. Magnetic resonance fingerprinting. Nature 495 (7440), 187–192. http://doi.org/10.1038/nature11971.

Meakin, J. a., Jezzard, P., 2013. An optimized velocity selective arterial spin labeling module with reduced eddy current sensitivity for improved perfusion quantification. Magn. Reson. Med. 69 (3), 832–838. http://doi.org/10.1002/mrm.24302.

Mora-Gutierrez, J.M., Garcia-Fernandez, N., Slon Roblero, M.F., Paramo, J.A., Escalada, F.J., Wang, D.J., et al., 2017. Arterial spin labeling MRI is able to detect early hemodynamic changes in diabetic nephropathy. J. Magn. Reson. Imag. http://doi.org/10.1002/jmri.25717.

Noguchi, T., Yoshiura, T., Hiwatashi, A., Togao, O., Yamashita, K., Nagao, E., Honda, H., 2012. Arterial spin-labelin magnetic resonance imaging: the timing of regional maximal perfusion-related signal intensity revealed by a multiphase technique. Jpn. J. Radiol. 30 (2), 137–145. http://doi.org/10.1007/s11604-011-0025-8.

Norris, D.G., Schwarzbauer, C., 1999. Velocity selective radiofrequency pulse trains. J. Magn. Reson. (San Diego, Calif. 1997) 137, 231–236. http://doi.org/10.1006/jmre.1998.1690.

Obara, M., Togao, O., Yoneyama, M., Okuaki, T., Shibukawa, S., Honda, H., Van Cauteren, M., 2016. Acceleration-selective arterial spin labeling for intracranial MR angiography with improved visualization of cortical arteries and suppression of cortical veins. Magn. Reson. Med. 0, 1–9. http://doi.org/10.1002/mrm.26275.

Parkes, L.M., 2005. Quantification of cerebral perfusion using arterial spin labeling: two-compartment models. J. Magn. Reson. Imag. 22 (6), 732–736. http://doi.org/10.1002/jmri.20456.

Pauls, M.M.H., Clarke, N., Trippier, S., Betteridge, S., Howe, F.A., Khan, U., et al., 2017. Perfusion by Arterial Spin labelling following Single dose Tadalafil In Small vessel disease (PASTIS): study protocol for a randomised controlled trial. Trials 18 (1), 229.

Perthen, J.E., Bydder, M., Restom, K., Liu, T.T., 2008. SNR and functional sensitivity of BOLD and perfusion-based fMRI using arterial spin labeling with spiral SENSE at 3 T. Magn. Reson. Imag. 26 (4), 513–522. http://doi.org/10.1016/j.mri.2007.10.008.

Petr, J., Schramm, G., Hofheinz, F., Langner, J., Van Den Hoff, J., 2013. Partial volume correction in arterial spin labeling using a Look-Locker sequence. Magn. Reson. Med. 70 (6), 1535–1543. http://doi.org/10.1002/mrm.24601.

Pruessmann, K.P., Weiger, M., Scheidegger, M.B., Boesiger, P., 1999. SENSE: sensitivity encoding for fast MRI. Magn. Reson. Med. 42 (5), 952–962. http://doi.org/10.1002/(SICI)1522-2594(199911)42:5<952::AID-MRM16>3.0.CO;2-S.

Qin, Q., Shin, T., Schär, M., Guo, H., Chen, H., Qiao, Y., 2015. Velocity-selective magnetization-prepared non-contrast-enhanced cerebral MR angiography at 3 tesla: improved immunity to b0/b1 inhomogeneity. Magn. Reson. Med. 0 n/a-n/a. http://doi.org/10.1002/mrm.25764.

Qin, Q., van Zijl, P.C.M., 2016. Velocity-selective-inversion prepared arterial spin labeling. Magn. Reson. Med. 76 (4), 1136–1148. http://doi.org/10.1002/mrm.26010.

Restom, K., Behzadi, Y., Liu, T.T., 2006. Physiological noise reduction for arterial spin labeling functional MRI. NeuroImage 31 (3), 1104–1115. http://doi.org/10.1016/j.neuroimage.2006.01.026.

Richter, X.V., Helle, X.M., Osch, X. M. J. P. Van, Lindner, X.T., Gersing, X.A.S., Tsantilas, X.P., et al., 2017. ADULT BRAIN MR Imaging of Individual Perfusion Reorganization Using Superselective Pseudocontinuous Arterial Spin-labeling in Patients with Complex Extracranial Steno-occlusive Disease, pp. 1–9.

Schmid, S., Ghariq, E., Teeuwisse, W.M., Webb, A., Van Osch, M.J.P., 2014. Acceleration-selective arterial spin labeling. Magn. Reson. Med. 71, 191–199. http://doi.org/10.1002/mrm.24650.

Schmid, S., Heijtel, D.F.R., Mutsaerts, H.J.M.M., Boellaard, R., Lammertsma, A.a, Nederveen, A.J., Osch, M.J.P.Van, March 18, 2015. Comparison of velocity and acceleration selective arterial spin labeling with 15 O H 2 O positron emission tomography. J. Cerebr. Blood Flow Metabol. 35 (8), 1296–1303. http://doi.org/10.1038/jcbfm.2015.42.

Schmithorst, V.J., Hernandez-Garcia, L., Vannest, J., Rajagopal, A., Lee, G., Holland, S.K., 2014. Optimized simultaneous ASL and BOLD functional imaging of the whole brain. J. Magn. Reson. Imag. 39, 1104–1117. http://doi.org/10.1002/jmri.24273.

St. Lawrence, K.S., Frank, J. a., Bandettini, P. a., Ye, F.Q., 2005. Noise reduction in multi-slice arterial spin tagging imaging. Magn. Reson. Med. 53 (3), 735–738. http://doi.org/10.1002/mrm.20396.

St. Lawrence, K.S., Owen, D., Wang, D.J.J., 2012. A two-stage approach for measuring vascular water exchange and arterial transit time by diffusion-weighted perfusion MRI. Magn. Reson. Med. 67 (5), 1275–1284. http://doi.org/10.1002/mrm.23104.

Su, P., Mao, D., Liu, P., Li, Y., Pinho, M.C., Welch, B.G., Lu, H., 2016. Multiparametric estimation of brain hemodynamics with MR fingerprinting ASL. Magn. Reson. Med. 0 (November), 1–12. http://doi.org/10.1002/mrm.26587.

Syrimi, Z.J., Vojtisek, L., Eliasova, I., Viskova, J., Svatkova, A., Vanicek, J., Rektorova, I., 2017. Arterial spin labelling detects posterior cortical hypoperfusion in non-demented patients with Parkinson's disease. J. Neural. Transm. 124 (5), 551–557.

Teeuwisse, W.M., Schmid, S., Ghariq, E., Veer, I.M., Van Osch, M.J.P., 2014. Time-encoded pseudocontinuous arterial spin labeling: basic properties and timing strategies for human applications. Magn. Reson. Med. 72 (6), 1712–1722. http://doi.org/10.1002/mrm.25083.

Van Gelderen, P., De Zwart, J. a., Duyn, J.H., 2008. Pittfalls of MRI measurement of white matter perfusion based on arterial spin labeling. Magn. Reson. Med. 59 (4), 788–795. http://doi.org/10.1002/mrm.21515.

Van Osch, M.J.P., Teeuwisse, W.M., Van Walderveen, M. a a, Hendrikse, J., Kies, D. a., Van Buchem, M. a, 2009. Can arterial spin labeling detect white matter perfusion signal? Magn. Reson. Med. 62 (1), 165–173. http://doi.org/10.1002/mrm.22002.

Vazquez, A.L., Fukuda, M., Tasker, M.L., Masamoto, K., Kim, S.-G., 2010. Changes in cerebral arterial, tissue and venous oxygenation with evoked neural stimulation: implications for hemoglobin-based functional neuroimaging. J. Cerebr. Blood Flow Metabol. Off. J. Int. Soc. Cerebr. Blood Flow Metabol. 30 (2), 428–439. http://doi.org/10.1038/jcbfm.2009.213.

Vazquez, A.L., Lee, G.R., Hernandez-Garcia, L., Noll, D.C., 2006. Application of selective saturation to image the dynamics of arterial blood flow during brain activation using magnetic resonance imaging. Magn. Reson. Med. 55 (4). http://doi.org/10.1002/mrm.20813.

von Samson-Himmelstjerna, F., Chappell, M.A., Sobesky, J., Günther, M., 2015. Subtraction free arterial spin labeling: a new Bayesian-inference based approach for gaining perfusion data from time encoded data. In: Proceedings of the International Society for Magentic Resonance in Medicine (ISMRM), p. 275.

von Samson-Himmelstjerna, F., Madai, V.I., Sobesky, J., Guenther, M., 2016. Walsh-ordered hadamard time-encoded pseudocontinuous ASL (WH pCASL). Magn. Reson. Med. 76 (6), 1814–1824. http://doi.org/10.1002/mrm.26078.

Wang, D.J.J., Alger, J.R., Qiao, J.X., Hao, Q., Hou, S., Fiaz, R., et al., 2012. The value of arterial spin-labeled perfusion imaging in acute ischemic stroke. Stroke 43 (4), 1018–1024.

Wang, J., Fernández-Seara, M. a, Wang, S., St Lawrence, K.S., 2007. When perfusion meets diffusion: in vivo measurement of water permeability in human brain. J. Cerebr. Blood Flow Metabol. Off. J. Int. Soc. Cerebr. Blood Flow Metabol. 27 (4), 839–849. http://doi.org/10.1038/sj.jcbfm.9600398.

Wells, J.A., Lythgoe, M.F., Gadian, D.G., Ordidge, R.J., Thomas, D.L., 2010. In vivo Hadamard encoded Continuous arterial spin labeling (H-CASL). Magn. Reson. Med. 63 (4), 1111–1118. http://doi.org/10.1002/mrm.22266.

Wierenga, C.E., Hays, C.C., Zlatar, Z.Z., 2014. Cerebral blood flow measured by arterial spin labeling MRI as a preclinical marker of Alzheimer's disease. J. Alzheim. Dis. 42 (s4), S411–S419.

Williams, D.S., Detre, J. a, Leigh, J.S., Koretsky, a P., 1992. Magnetic resonance imaging of perfusion using spin inversion of arterial water. Proc. Natl. Acad. Sci. Unit. States Am. 89 (1), 212–216. http://doi.org/10.1073/pnas.89.9.4220e.

Wolff, S.D., Balaban, R.S., 1989. Magnetization transfer contrast (MTC) and tissue water proton relaxation in vivo. Magn. Reson. Med. Off. J. Soc. Magn. Reson. Med. 10 (1), 135–144. http://doi.org/10.1002/mrm.1910100113.

Wong, E.C., 2007. Vessel-encoded arterial spin-labeling using pseudocontinuous tagging. Magn. Reson. Med. 58 (6), 1086–1091. http://doi.org/10.1002/mrm.21293.

Wong, E.C., Buxton, R.B., Frank, L.R., 1998. A theoretical and experimental comparison of continuous and pulsed arterial spin labeling techniques for quantitative perfusion imaging. Magn. Reson. Med. Off. J. Soc. Magn. Reson. Med. 40 (3), 348–355.

Wong, E.C., Cronin, M., Wu, W.-C., Inglis, B., Frank, L.R., Liu, T.T., 2006. Velocity-selective arterial spin labeling. Magn. Reson. Med. Off. J. Soc. Magn. Reson. Med. 55 (6), 1334–1341. http://doi.org/10.1002/mrm.20906.

Wong, E.C., Guo, J., 2012. Blind detection of vascular sources and territories using random vessel encoded arterial spin labeling. Magn. Reson. Mater. Phys. Biol. Med. 25 (2), 95–101. http://doi.org/10.1007/s10334-011-0302-7.

Wright, K.L., 2014. Theoretical framework for MR fingerprinting with ASL: simultaneous quantification of CBF, transit time, and T1. Ismrm 1, 1.

Wu, W.-C., Wong, E.C., 2007. Feasibility of velocity selective arterial spin labeling in functional MRI. J. Cerebr. Blood Flow Metabol. Off. J. Int. Soc. Cerebr. Blood Flow Metabol. 27 (4), 831–838. http://doi.org/10.1038/sj.jcbfm.9600386.

Xu, F., Ge, Y., Lu, H., 2009. Noninvasive quantification of whole-brain cerebral metabolic rate of oxygen (CMRO2) by MRI. Magn. Reson. Med. 62 (1), 141–148. http://doi.org/10.1002/mrm.21994.

Yamashita, K., Hiwatashi, A., Togao, O., Kikuchi, K., Yamaguchi, H., Suzuki, Y., et al., 2017. Cerebral blood flow laterality derived from arterial spin labeling as a biomarker for assessing the disease severity of Parkinson's disease. J. Magn. Reson. Imag. 45 (6), 1821–1826.

Yan, L., Li, C., Kilroy, E., Wehrli, F.W., Wang, D.J.J., 2012. Quantification of arterial cerebral blood volume using multiphase-balanced SSFP-based ASL. Magn. Reson. Med. 68 (1), 130–139. http://doi.org/10.1002/mrm.23218.

Ye, 2000. H(2)(15)O PET validation of steady-state arterial spin tagging cerebral blood flow measurements in humans. Magn. Reson. Med. 44 (3), 450–456. Retrieved from. http://www.ncbi.nlm.nih.gov/pubmed?term.

Ye, F.Q., Frank, J.A., Weinberger, D.R., McLaughlin, A.C., 2000b. Noise reduction in 3D perfusion imaging by attenuating the static signal in arterial spin tagging (ASSIST). Magn. Reson. Med. 44 (1), 92–100. http://doi.org/10.1002/1522-2594(200007)44:1<92::AID-MRM14>3.0.CO;2-M.

Zaharchuk, G., El Mogy, I.S., Fischbein, N.J., Albers, G.W., 2012. Comparison of arterial spin labeling and bolus perfusion-weighted imaging for detecting mismatch in acute stroke. Stroke 43 (7), 1843–1848.

Zhang, W., Silva, a. C., Williams, D.S., Koretsky, a. P., 1995. NMR measurement of perfusion using arterial spin labeling without saturation of macromolecular spins. Magn. Reson. Med. 33 (3), 370–376. http://doi.org/10.1002/mrm.1910330310.

Zhang, X., Ghariq, E., Hartkamp, N.S., Webb, A.G., Van Osch, M.J.P., 2016. Fast cerebral flow territory mapping using vessel encoded dynamic arterial spin labeling (VE-DASL). Magn. Reson. Med. 75 (5), 2041–2049. http://doi.org/10.1002/mrm.25806.

Zhou, J., Wilson, D.A., Ulatowski, J.A., Traystman, R.J., van Zijl, P.C.M., 2001. Two-compartment exchange model for perfusion quantification using arterial spin tagging. J. Cerebr. Blood Flow Metabol. 21 (4), 440–455. http://doi.org/10.1097/00004647-200104000-00013.

Zimmer, F., Zöllner, F.G., Hoeger, S., Klotz, S., Tsagogiorgas, C., Krämer, B.K., Schad, L.R., 2013. Quantitative renal perfusion measurements in a rat model of acute kidney injury at 3T: testing inter- and intramethodical significance of ASL and DCE-MRI. PLoS One 8 (1). http://doi.org/10.1371/journal.pone.0053849.